



Modelling the effect of BIPV window in the built environment: Uncertainty and sensitivity

Liutao Chen ^a, Jiachuan Yang ^{a,*}, Peiyuan Li ^b

^a Department of Civil and Environmental Engineering, The Hong Kong University of Science and Technology, Hong Kong, China

^b School of Sustainable Engineering and the Built Environment, Arizona State University, Tempe, USA



ARTICLE INFO

Keywords:

BIPV window

Urban heat island

Building energy efficiency

Power generation

ABSTRACT

BIPV (building-integrated photovoltaic) window has been proven as a promising technology to increase renewable energy and reduce environmental effects of the building. The effect of BIPV window in the built environment could change significantly with the window configuration, building materials, and urban landscape, which have a large variability within cities. In this study, we adopted a newly developed building energy model coupled with a single-layer urban canopy model (BEM-SLUCM) to characterize the uncertainties of BIPV window effect at the neighbourhood scale in a hot desert climate city, Phoenix, USA. Using an advanced Markov chain Monte Carlo algorithm, extensive simulations were conducted to quantify the sensitivity of extreme outdoor microclimate, building cooling load and renewable energy generation to various input parameters. Results show that the canyon aspect ratio, window coverage, and power generation efficiency are pivotal to maximize the electricity generation by BIPV window. Canyon air temperature and building cooling load are highly sensitive to momentum roughness length above canyon, thickness of building envelope, air conditioning setpoint temperature, and canyon aspect ratio. This indicates a strong dynamic interaction between building's indoor space and the surrounding canyon environment. In contrast, thermal and optical properties of BIPV window have negligible effects on the urban thermal environment. Findings in this study reveal key mechanisms that regulate the urban microclimate and building energy consumption, provide guidance for BIPV applications in the built environment, and shed new lights on the sustainable design of urban neighbourhoods.

1. Introduction

According to the United Nations, 55% of global population lives in urban areas in 2018 and the percentage is expected to grow to 68% by 2050 [1]. The unprecedented growth rate of urban population stimulates the construction of buildings to meet the housing demand. Increased number of buildings is accompanied by elevated energy consumption in the past decades, which has intensified the urban heat island effect and posed threats to urban energy supply systems [2]. In 2019, the building sector was responsible for 30% of global final energy use, and building-related CO₂ emissions reached an all-time high [3]. To achieve the sustainable low carbon future goal set by the Paris Agreement, it is imperative to introduce renewable energy technologies into cities for enhancing building energy efficiency.

With the ability to convert solar energy into electricity, photovoltaic (PV) cell is one of the most reliable renewable energy technologies that has been widely deployed in recent years [4]. Within cities,

building-integrated photovoltaic (BIPV) technology is a prominent solution for buildings to achieve zero-energy and carbon neutrality [5,6]. BIPV system does not occupy valuable land sources and has a modern appearance that suits architectural design. These advantages make BIPV technology one of the fastest growing segments of the PV market [4]. Considering future cost reduction and continuous policy support [7,8], solar PV is projected to account for 60% of all renewable energy capacity additions through 2025, especially in China, Europe, and the US [9].

BIPV window is one important component of the BIPV system [10]. Major types of BIPV window include non-ventilated air-filled BIPV window [11,12], ventilated BIPV window [13,14], BIPV-vacuum glazing [15,16], etc. Solar cells in existing BIPV window products are mainly fabricated by crystalline silicon (c-Si, including mono and poly types) or by the thin-film technology. Crystalline silicon solar cells, the first-generation technology, exhibit high durability and conversion efficiency, but have large manufacturing costs and generate substantial silicon waste in production process [10]. In comparison, the thin-film

* Corresponding author.

E-mail address: cejyang@ust.hk (J. Yang).

technology based BIPV window has low manufacturing costs, weak temperature-dependent performance, and high flexibility in the integration with building design [10]. These characteristics make thin-film solar cells receive increasing attention in BIPV applications, especially under hot and warm climate [17], which is the focus of this study.

Compared with traditional clear glass window, BIPV window has a better thermal insulation and a lower solar heat gain, which can decrease the cooling load but may increase the heating load of buildings [18–20]. BIPV window is thus advantageous in cooling-dominated low latitude cities [20,21]. In Houston under the humid subtropical climate, the installation of BIPV windows in a code-compliant single-story residential building could save the annual cooling load by 10.4%–25.9% [22]. Under the hot dry climate in United Arab Emirates, Salameh et al. [23] found that the annual air conditioning electricity consumption of a 3-stoery commercial building can save about 17% after replacing normal glass windows by BIPV windows, whilst the power generation can offset more than 10% of the energy demand. These existing studies, however, mainly focus on the impact of BIPV window on the energy consumption of a standalone building. The effect of BIPV window in the built environment, e.g., modifying the diurnal variation of urban heat island, under dynamic interactions with the indoor space and outdoor urban environment, has been rarely investigated due to the difficulty of conducting full-scale experiments and the lack of modelling tools.

To fill the research gap, Chen et al. [24] recently developed a parameterization scheme for non-ventilated transparent amorphous silicon BIPV window, and incorporated it into a building energy model coupled with a single-layer urban canopy model (BEM-SLUCM). The single-layer urban canopy model (SLUCM) features a representation of complex urban surface processes, including urban vegetation (e.g., green roof [25], irrigated lawn [26], and tree [27]), CO₂ exchange [28], and usage of engineering materials [29]. The coupled model enables the evaluation of BIPV window performance at the neighbourhood scale (i.e., inside street canyons) for the first time. The presence of BIPV windows modifies the urban energy budget mainly through two processes: (1) Temperature characteristics of BIPV window alter the heat exchange between building façade and canyon air; (2) Solar heat gain and power generation of BIPV window regulate the indoor cooling load, and subsequently change the amount of waste heat released from the building into the outdoor urban canyon. Modelling the effect of BIPV window nevertheless remains challenging as input parameters, e.g., canyon morphology and material properties, have a large spatial variety in the heterogeneous built environment. Inaccurate determination of input parameters can result in substantial errors, but a complete set of input parameters is rarely available due to the limited field measurements. This calls for the investigation of the model's sensitivity to various input parameters: the impact of an uncertain parameter on a model output can be estimated by changing its value while fixing other parameters. This conventional approach for sensitivity analysis has been adopted in previous studies [30–32]. Such approach is nevertheless biased by the choice of the control scenario, and the computational cost increases exponentially with the dimension of the uncertain parameter space. As a result, it is hard to capture the statistically least probable case of the model output, viz., extreme events such as the hottest canyon and the largest building cooling demand when applying BIPV window. These extreme events have detrimental impacts on pedestrians' thermal comfort and energy supply system, and design/material parameter that leads to the worst conditions shall be avoided at the planning stage.

To overcome aforementioned limitations, stochastic algorithms have been developed to characterize sensitivity of models involving large dimensionality and complex dynamics [33,34]. One specific method has been applied for sensitivity analysis of SLUCM [25,35,36] is the advanced Markov chain Monte Carlo (MCMC) algorithm. The MCMC approach achieves small probability events as a product of large probability events by introducing a sequence of intermediate sampling, and significantly improves the efficiency of generating conditional samples of small probability [34]. Results in Princeton, New Jersey and Phoenix,

Arizona showed that urban energy fluxes and surface temperatures are highly sensitive to the variations in canyon geometry, but are insensitive to material emissivity and building indoor temperature [36]. Thermal properties of roof materials are also found to have critical impacts on regulating the urban energy fluxes. However, these findings were based on the SLUCM version without building energy simulations. A reassessment of the uncertainty and sensitivity of the coupled BEM-SLUCM model is essential after the implementation of BIPV window and building energy simulations.

In this study, we adopted the coupled BEM-SLUCM model to quantify the uncertainty associated with the effect of transparent amorphous silicon BIPV windows in a fully interactive built environment. The city of Phoenix, Arizona, USA is selected as the study site given its hot desert climate favours the power generation by BIPV windows. We aim to address two major research questions for an urban canyon with BIPV windows under summer clear days: 1) What are the key parameters that regulate the power generation, building cooling load, and outdoor microclimate?, and 2) What are the magnitudes of power generation, building cooling load, and outdoor microclimate under the best/worst case? By using the MCMC approach, we aim to reveal the ubiquitous parameter uncertainties related to the effect of BIPV windows through a statistical quantification of model sensitivity. The findings are expected to promote the understanding of the interplay among renewable energy technology, urban microclimate, and building indoor environment. The rest of this paper is organized as follows: Section 2 describes the methodology, including the coupled BEM-SLUCM model, the advanced Markov chain Monte Carlo simulation, and the statistics of uncertain parameters. Sensitivity of monitored model outputs to uncertain parameters and implications for urban neighbourhood design are discussed in Section 3. Conclusions are presented in Section 4.

2. Methodology

2.1. BEM-SLUCM

In this section, the newly developed BEM-SLUCM model is briefly explained, and detailed description of the governing equations can be found in the previous study [24]. The schematic of the coupled BEM-SLUCM model is shown in Fig. 1. An urban neighbourhood is represented as a canyon with buildings of the same height on two sides of the road. The energy balance equation for the urban canopy layer is given by:

$$R_{net} + Q_{AC} = QH_u + QLE_u + G \quad (1)$$

where R_{net} is the net radiation, Q_{AC} is the waste heat released from the air conditioning (A/C) of the buildings, QH_u and QLE_u are the turbulent sensible and latent heat fluxes from the entire urban surface, and G is the conductive heat exchanges with the substrates. The BEM-SLUCM calculates the energy balance at the rooftop height and within the canopy layer. Using forcing data measured at the height of two to five times the building height, the sensible and latent heat exchange (QH_u and QLE_u in Eq. (1)) between the urban surface and overlying inertial sublayer is computed. The BEM-SLUCM diagnoses the canyon air temperature (T_{can}) based on the sensible heat fluxes from road, wall, window surfaces (excluding roof surface), ventilation heat exchange from buildings, and the waste heat released by A/C. It should be noted that in SLUCM, the atmospheric layer occupied by the buildings is treated as a whole layer. Therefore, the calculated T_{can} is the mean temperature of the air within the entire canyon. Average turbulent heat fluxes over road/wall/window surfaces are calculated, and vertical discretization of incident radiation on BIPV window at different heights is not resolved. To investigate the impact of BIPV window at different heights in the urban canyon, incorporation of the BIPV window scheme into multi-layer models is necessary.

The meteorological condition in the canyon is solved by SLUCM, while the building energy model (BEM) calculates dynamic sensible and

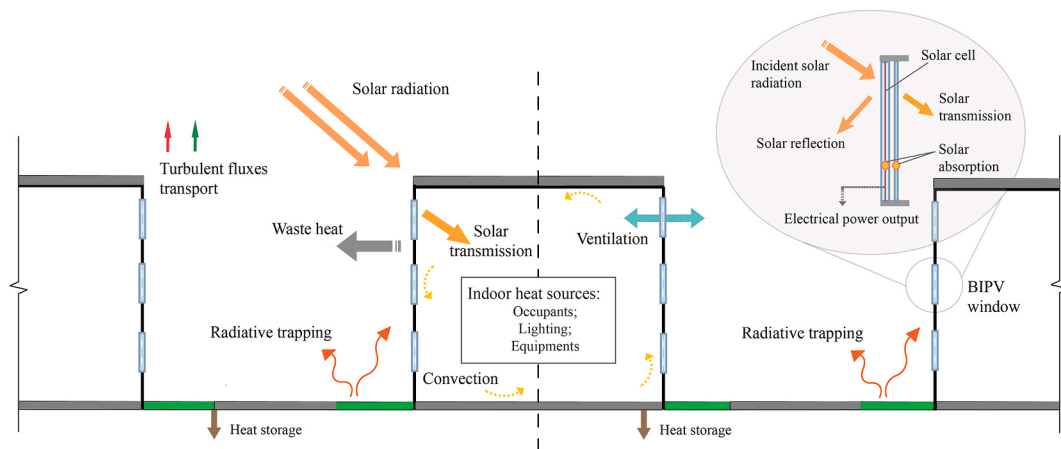


Fig. 1. Schematic of the energy transport in the coupled BEM-SLUCM. Simulations are conducted for one street canyon, i.e., either the left- or right-hand side of the dashed line at any given time. The two-canyon juxtaposition here is for illustration purposes only.

latent heat loads inside the building, including the convective heat exchange between interior surfaces and indoor air, ventilation heat exchange, and the heat loads caused by occupants, lighting and electric equipment. Other energy-consuming components in the building, such as water heating and cooking, are neglected in the model as they account for a limited portion of the total energy use. To examine the impact of BIPV window applications at the region scale in the future, the BIPV window scheme is incorporated into the SLUCM [24], which has high computational efficiency when coupled with mesoscale climate models. Nevertheless, the BEM simplifies buildings as single boxes and neglects the heat exchange between floors, which brings potential errors when simulating multi-floor high-rise buildings. To maintain indoor air temperature at a comfortable level, the total sensible and latent heat loads (i.e., cooling load) that need to be pumped out from the building are estimated. The energy required to operate A/C to transport the heat outdoor, together with the cooling load, will be released as the source term Q_{AC} for the canyon (see Eq. (1)). Through this process, the urban canopy model and building energy model are two-way coupled, which can solve the dynamics of heat and moisture transport in the built environment.

In this study, we focus on the impact of non-ventilated amorphous silicon BIPV double-pane windows, which are composed of a single plate PV module, air cavity, and a clear glass (see Fig. 1). The single plate PV module is an assembly of non-crystalline transparent thin-film solar cells, which are sandwiched between two sheets of clear glass. The non-ventilated BIPV window is modelled using a six-boundary parameterization scheme, i.e., the outer, middle, and inner surfaces of the front and rear panes. Heat emitted by the solar cells is considered in the longwave radiative heat exchange and conduction terms in the window parameterization scheme. The capacity of the scheme in simulating window surface temperature and power generation has been evaluated against a mock-up model experiment in our previous study [24]. As shown in Fig. 1, incoming solar radiation can be reflected by, absorbed by, and transmit through the BIPV window. The respective portions are determined by the incidence angle and window optical properties. Solar cells of the BIPV window convert the incoming solar radiation into electric output. The power generation varies with the incidence angle of solar irradiance:

$$P = SR\tau_{PV}(\theta)IAM(\theta)A_{PV}\eta_{PV}, \quad (2)$$

where SR is the solar irradiance (W m^{-2}) incident on the outer window surface, $\tau_{PV}(\theta)$ is the angle-dependent transmittance of the PV module [37]. IAM is the incident angle modifier to account for the angle of incidence (θ)'s influence on the power output, which is an empirical relationship [38]. A_{PV} is the area (m^2) of the PV module. η_{PV} is the PV module's electrical efficiency, which is a function of the operating

temperature of the PV cell (T_{cell}) [39,40]:

$$\eta_{PV} = \eta_{ref} [1 - \beta_{ref} (T_{cell} - T_{ref})], \quad (3)$$

where η_{ref} and β_{ref} , normally given by the PV manufacturer, are the reference electrical efficiency (%) and temperature coefficient ($^{\circ}/^{\circ}\text{C}$) under standard test conditions at the reference temperature $T_{ref} = 25^{\circ}\text{C}$ [41]. A positive (negative) β_{ref} indicates the power generation efficiency decreases (increases) with the PV module temperature. Crystalline silicon (c-Si) PV modules have positive β_{ref} , whereas amorphous silicon (a-Si) modules show lower or slightly negative β_{ref} [41]. The cell temperature is calculated by the six-boundary BIPV window parameterization scheme, which captures the indoor-outdoor heat exchange through BIPV windows. After implementation of the BIPV window scheme into BEM-SLUCM, outdoor microclimate, indoor energy consumption, and the BIPV window dynamically interact with each other and jointly regulate the urban thermal environment.

2.2. Advanced Markov chain Monte Carlo simulation

To assess the impact of BIPV window in the built environment, we chose to monitor the daily maximum canyon air temperature (T_{can}^{max} in $^{\circ}\text{C}$), daily minimum canyon air temperature (T_{can}^{min} in $^{\circ}\text{C}$), daily total building cooling load (CL_{tot} in kWh), and daily total power generation of BIPV window (P_{tot} in kWh) as critical responses. These responses can inform us the outdoor thermal environment and building energy consumption associated with the environmental sustainability of an urban neighbourhood. The theoretical basis of MCMC algorithm is to construct a Markov chain, which proceeds by randomly walking through the searching space and converges to a distribution that tends to yield larger monitored outputs. By converting the small probability problem to a sequence of more frequent problems, the rare events can be estimated with a small set of simulations [34]. By using the MCMC method, here we quantified the impact of uncertain input parameters on monitored outputs, and identified key parameters that lead to extremely high T_{can}^{max} , T_{can}^{min} , CL_{tot} , and P_{tot} . The exceedance probability $p(Y > y)$ is defined as the probability of a critical response Y exceeding a threshold level y ; i.e., at what probability a certain value y will be exceeded for a monitored model output. A smaller exceedance probability p indicates a more extreme event.

The procedure of the sensitivity analysis in this study is described as follows (see Fig. 2). Before the simulation procedure, the number of conditional levels (N), the conditional probability at each level (p_1, p_2, \dots, p_N), the number of simulations at each level (n), and the monitored outputs Y were defined. First, we selected X uncertain parameters of interest and chose a proper probability distribution function (PDF) for

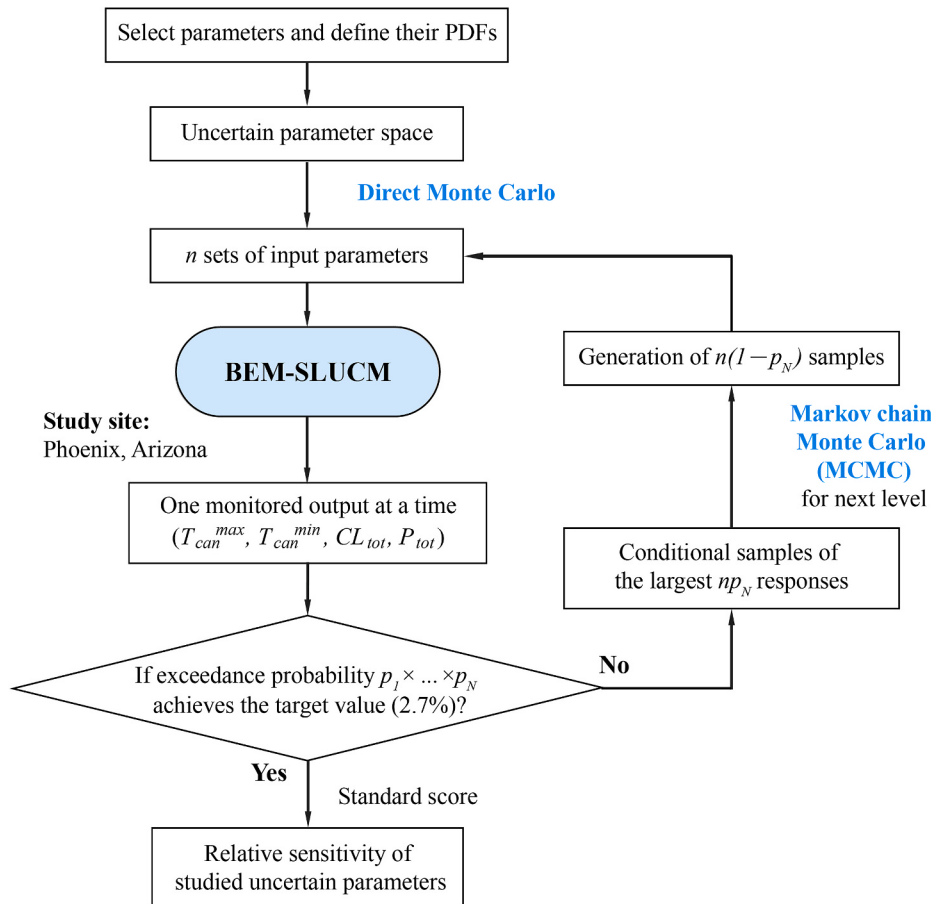


Fig. 2. Flowchart of the sensitivity analysis using the advanced Markov chain Monte Carlo algorithm.

each parameter. This generated a parameter space at the initial stage. Direct Monte Carlo (DMC) was then performed to create a set of input parameters for the BEM-SLUCM following the prescribed PDFs. In each simulation, BEM-SLUCM imported one set of X parameters to model the impact of BIPV window and monitored outputs Y (i.e., T_{can}^{max} , T_{can}^{min} , CL_{tot} , and P_{tot}) were recorded. At each level, the values of Y from n simulations were ranked in an ascending order. Given the conditional probability p_1 , the threshold value y_1 of the first conditional level was determined as the np_1 -th largest value of Y among the n simulations. Utilizing the sets of parameters that produced the largest np_1 responses (conditional samples at the first level) as seeds, additional $n(1 - p_1)$ samples were generated using the MCMC algorithm to make up a total of n samples for the next level of simulation. This algorithm continued at higher levels until the monitored outputs reached the target exceedance probability $p_{target} = p_1 \times p_2 \times \dots \times p_N$. Note that individual monitored outputs have different responses to the same uncertain parameter space, and thus the sensitivity analysis was conducted for each monitored output separately.

In this study, we set three conditional levels ($N = 3$) and an identical conditional probability $p = 0.3$ for all levels. This meant the MCMC algorithm achieved the highest 30% of one monitored output at each conditional level, and the final target exceedance probability was 2.7% (0.3^3). At each level, we conducted 500 simulations ($n = 500$), and as a result we had 1550 simulations for a single sensitivity analysis (500 simulations for the first level, and 350 simulations for each of the next three levels). To enhance the statistical significance, we conducted 50 independent runs (i.e., $N_{run} = 50$) for each monitored output Y , namely, T_{can}^{max} , T_{can}^{min} , CL_{tot} , and P_{tot} . The major advantage of the MCMC algorithm is its efficient in capturing the tail of the probability distributions when various uncertain parameters change simultaneously. In this

study, a total of 310000 simulations (1550 simulations per run \times 50 runs per output \times 4 output) were carried out. To achieve the same exceedance probability during the sensitivity analysis, a conventional approach will require 6200000 simulations (1000 simulations to capture the 2.7% extreme event per parameter \times 31 uncertain parameters \times 50 runs per output \times 4 output), whose computational cost is 20 times larger.

The distribution of the conditional samples at different levels was used to determine the sensitivity of the monitored outputs to individual parameters. A large deviation of the conditional sample distribution from the predefined distribution suggests a high sensitivity of the monitored output to studied uncertain parameter. We adopted the Standard Score (SS) to calculate the deviation of the conditional sample distribution from the predefined distribution:

$$SS = \frac{1}{N} \sum_{j=1}^N \frac{E[X|Y > y_j] - E[X]}{\sigma[X]}, \quad (4)$$

where $E[X|Y > y_j]$ is the expected value of parameter X at conditional level j , $E[X]$ is the prescribed mean of unconditional distribution of the parameter, y_j is the critical response at conditional level j , and $\sigma[X]$ is the prescribed standard deviation of the parameter. A standard score with absolute value lower than 0.15 (i.e., $|SS| < 0.15$) indicates that the mean value of conditional samples is within 0.15 standard deviation from the prescribed mean. This suggests that the monitored output is insensitive to the input parameter. On the other hand, a large $|SS|$ denotes strong sensitivity, as the skewness of conditional samples contributes to high exceedance probabilities. In this study, we defined “ $0.15 \leq |SS| < 0.3$ ” as slightly sensitive, “ $0.3 \leq |SS| < 0.5$ ” as moderately sensitive, “ $0.5 \leq |SS| < 0.75$ ” as very sensitive, and “ $0.75 \leq |SS|$ ” as extremely sensitive. A positive (negative) SS implies that increasing the value of input parameter results in an increase (decrease) of the monitored output.

2.3. Uncertain parameter space

We proposed to analyse a total of 31 uncertain parameters in this study. The statistics of individual parameters are summarized in Table 1. Focused on the impact of BIPV window, we excluded parameters related to outdoor natural landscape (e.g., tree and irrigated lawn). Table 1 contains 16 parameters related to the dimensional, thermal, optical, and electrical properties of BIPV window. For simplicity and computational efficiency, we assumed a usage of homogeneous materials over individual urban facets. As a result, thermal properties of the roof/wall/indoor ground remained constant at different depths.

The choice of PDF governs the efficiency of generating conditional samples. Following previous studies, we adopted normal distributions for thermal properties of engineering materials. The standard deviations were set to be 25% of the mean value [36], except for window emissivity and A/C setpoint temperature, whose values were manually decided in accordance with the realistic range. In terms of dimensional properties, uniform distributions were assigned for morphological surface parameters, thickness of roof/wall/window, and roughness lengths. Their possible values in Table 1 all lie within a physically feasible range with references to the literature. The canyon aspect ratio had a wide range from 0.2 to 5, and covered typical urban neighbourhoods for all the built local climate zone types [45]. The roughness length of heat was assumed to be one tenth of the momentum roughness length [46] for both the canyon and the roof. We did not examine the sensitivity of model responses to the angle-dependent transmittance, absorptance, and reflectance separately as their summation is one. Because the uncertainty associated with each parameter is stochastic and shall be independent of each other, only the effective absorptance of the front PV module and the rear pane were included in the analysis.

2.4. Numerical experiment

In this study, the BEM-SLUCM was driven by the meteorological forcing data at the height of 22.1 m above the ground level from the eddy covariance tower in a residential suburban of Phoenix, Arizona [47]. Located at southwest US, Phoenix has a desert climate type with extremely hot summers. The abundant sunshine resources make Phoenix one of the most favourable sites for BIPV application [20]. To investigate the maximum BIPV impact, the BEM-SLUCM model was run for one-day on 15 June 2012 after a two-day spin-up period (see Fig. 3). Given the massive number of simulations (i.e., 310000 simulations) in this study, a short simulation period is essential for computational efficiency. We selected 15 June to represent the meteorological conditions under a clear sky during the dry pre-monsoon summertime. During the pre-monsoon period in Phoenix, strong solar radiation can maximize the impact of BIPV window, and day-to-day variation of meteorological forcing is small. Under this circumstance, urban landscape and building properties have dominant effects (as compared to meteorological forcing) on outdoor microclimate and building energy consumption. The one-day study period of 15 June was chosen to efficiently estimate the key parameters that regulate the power generation, building cooling load, and outdoor microclimate for an urban canyon with BIPV windows under summer clear days. In all simulations, we considered a single-storey residential building (10 m height × 11.25 m width × 11.25 m length) with an identical occupant schedule (Table 2 of Ref. [24] based on the guidelines of US Department of Energy) to allow a direct comparison of the response of building cooling load.

Before the MCMC simulation, the performance of BEM-SLUCM in capturing the energy balance of the study site in Phoenix was evaluated. Simulated net radiation (R_{net}), sensible heat flux (H_u), and latent heat flux (LE_u) were compared against hourly field measurements from the

Table 1
Statistics of studied uncertain parameters in this study.

Parameters	Symbol	Unit	PDF	Min	Max	Mean	S.d.
<i>BIPV window properties</i>							
Window-to-wall ratio	WWR	-	Uniform	0	1		
Width of PV panel	W_{WD}	m	Uniform	0.4	1.5		
Height of PV panel	H_{WD}	m	Uniform	0.5	1.8		
PV module thickness	d_{PV}	m	Uniform	0.002	0.02		
Air cavity thickness [42]	d_{Cav}	m	Uniform	0.001	0.03		
Rear clear glass thickness	d_{cg}	m	Uniform	0.002	0.02		
PV module thermal conductivity	k_{PV}	$\text{W m}^{-1} \text{K}^{-1}$	Normal	0.4	2	1	0.25
Rear clear glass thermal conductivity	k_{cg}	$\text{W m}^{-1} \text{K}^{-1}$	Normal	0.6	2	1	0.25
Heat capacity of PV module	C_{PV}	$\text{J K}^{-1} \text{m}^{-2}$	Normal	1500	4500	2700	675
Heat capacity of rear clear glass	C_{cg}	$\text{J K}^{-1} \text{m}^{-2}$	Normal	1000	3000	2000	500
PV module emissivity	ϵ_{PV}	-	Normal	0.7	0.98	0.84	0.084
Rear clear glass emissivity [43]	ϵ_{cg}	-	Normal	0.7	0.98	0.84	0.084
PV module effective absorptance [44]	a_{PV}	-	Normal	0.35	0.95	0.75	0.1875
Rear clear glass effective absorptance	a_{cg}	-	Normal	0.02	0.25	0.08	0.02
Reference electrical efficiency [40]	η_{ref}	%	Normal	3	30	12	3
Temperature coefficient [40]	β_{ref}	$^{\circ}/^{\circ}\text{C}$	Normal	-0.5	0.8	0.45	0.1125
<i>Wall properties</i> [36]							
Albedo	a_w	-	Normal	0	1	0.25	0.0625
Thermal conductivity	k_w	$\text{W m}^{-1} \text{K}^{-1}$	Normal	0.2	2	1.3	0.325
Heat capacity	C_w	$\text{MJ m}^{-3} \text{K}^{-1}$	Normal	0.1	4	1.26	0.315
Thickness	d_w	m	Uniform	0.1	0.8		
<i>Roof properties</i> [36]							
Albedo	a_R	-	Normal	0	1	0.15	0.0375
Thermal conductivity	k_R	$\text{W m}^{-1} \text{K}^{-1}$	Normal	0.2	3	1.2	0.3
Heat capacity	C_R	$\text{MJ m}^{-3} \text{K}^{-1}$	Normal	0.1	4	1.52	0.380
Thickness	d_R	m	Uniform	0.1	0.8		
Roughness length for momentum above roof	Z_{mR}	m	Uniform	0.0001	0.2		
<i>Indoor ground properties</i> [36]							
Thermal conductivity	k_{Gi}	$\text{W m}^{-1} \text{K}^{-1}$	Normal	0.2	3	1.7	0.425
Heat capacity	C_{Gi}	$\text{MJ m}^{-3} \text{K}^{-1}$	Normal	0.1	4	2.10	0.525
<i>Others</i>							
A/C setpoint temperature [36]	T_B	$^{\circ}\text{C}$	Normal	20	28	24	1.0
Canyon aspect ratio	h/w	-	Uniform	0.2	5		
Canyon orientation	θ_{can}	rad	Uniform	0	π		
Roughness length for momentum above canyon [36]	Z_{mc}	m	Uniform	0.01	2		

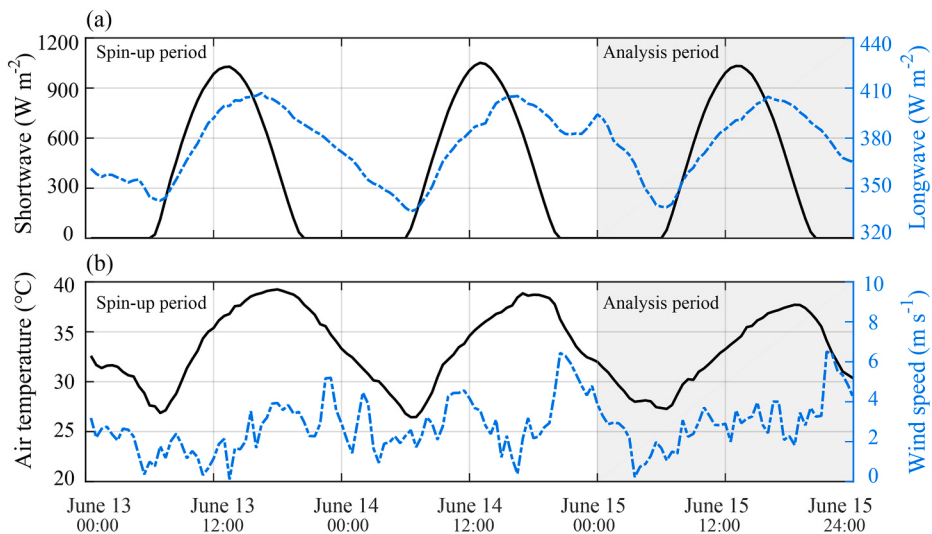


Fig. 3. Atmospheric forcing measurements for the BEM-SLCUM model from June 13 to 15, 2012 by the eddy covariance tower in Phoenix. (a) shortwave and longwave radiation; (b) air temperature and wind speed. Only the results in the shaded period are analysed in this study.

eddy covariance tower [47]. Fig. 4 shows that simulated R_{net} is in good agreement with the observations, with a coefficient of determination (R^2) of 0.99 and a root-mean-square-error (RMSE) of 20.1 W m^{-2} . The model slightly overestimates H_u at night and underestimates LE_u around noontime. Such biases are within an acceptable range [48], with a RMSE of 46.4 W m^{-2} for H_u and a RMSE of 20.3 W m^{-2} for LE_u . Overall, the BEM-SLCUM model can capture the urban energy balance during the study period with a reasonable accuracy, which lays a solid foundation for subsequent sensitivity analysis. A complete evaluation of the performance of the BEM-SLCUM model can be found in the previous study [24].

3. Results and discussion

3.1. Statistical convergence

The Markov chain Monte Carlo simulation in this study involves stochastic processes, and the sensitivity of monitored outputs to individual uncertain parameters can have a large variability from run to run. Taking the average of multiple runs is essential for obtaining a meaningful sensitivity result, yet it is unclear how many runs is sufficient. To examine the statistical convergence of the sensitivity analysis, we computed the coefficient of variation (CV) using the SS results from 50 independent runs. CV is defined as the ratio of standard deviation over

mean, and it has been widely used to measure the dispersion or variability of dataset. Note that for parameters with mean SS values close to zero, CV will approach infinity. We therefore only plot the relationship between CV and the number of runs for sensitive parameters ($|SS| > 0.15$) in Fig. 5. Fig. 5 shows that the magnitude of CV decreases gradually with increased N_{run} and becomes stable at $N_{run} = 40$ for most parameters, indicating a statistical convergence for SS values. One exception is the CV for A/C setpoint temperature TB in Fig. 5a. The CV curve decreases and reaches an inflection point of -25% at $N_{run} = 15$, then increases slowly to a value of about -18% at $N_{run} = 50$. Mean SS of TB increases rapidly from -0.27 to -0.14 when N_{run} increases from 1 to 10, then it becomes steady at around -0.15 (results not shown here). The mean SS values for all studied parameters are stable when N_{run} is greater than 30. This confirms that 50 independent runs in this study are sufficient to derive representative SS results for model's sensitivity to uncertain input parameters.

3.2. Exceedance probability of monitored outputs

Simulated model responses of T_{can}^{max} , T_{can}^{min} , CL_{tot} , and P_{tot} with BIPV window applications in the street canyon are examined in this section. The monitored outputs at different exceedance probabilities averaged over 50 runs are shown in Fig. 6. The threshold values of T_{can}^{max} with the exceedance probability of 30%, 9%, and 2.7% are

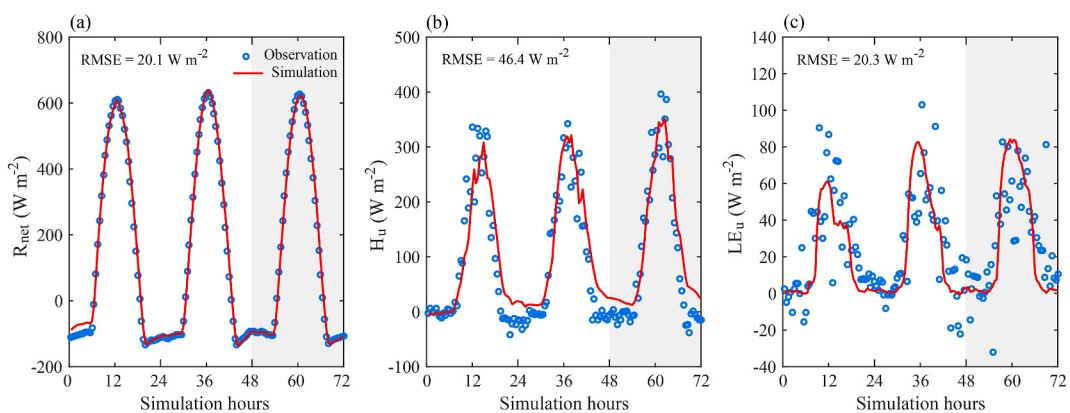


Fig. 4. Comparison of observed and simulated (a) net radiation, (b) sensible heat, and (c) latent heat flux over the study site in Phoenix from June 13 to 15, 2012. The shaded area denotes the study period for sensitivity analysis.

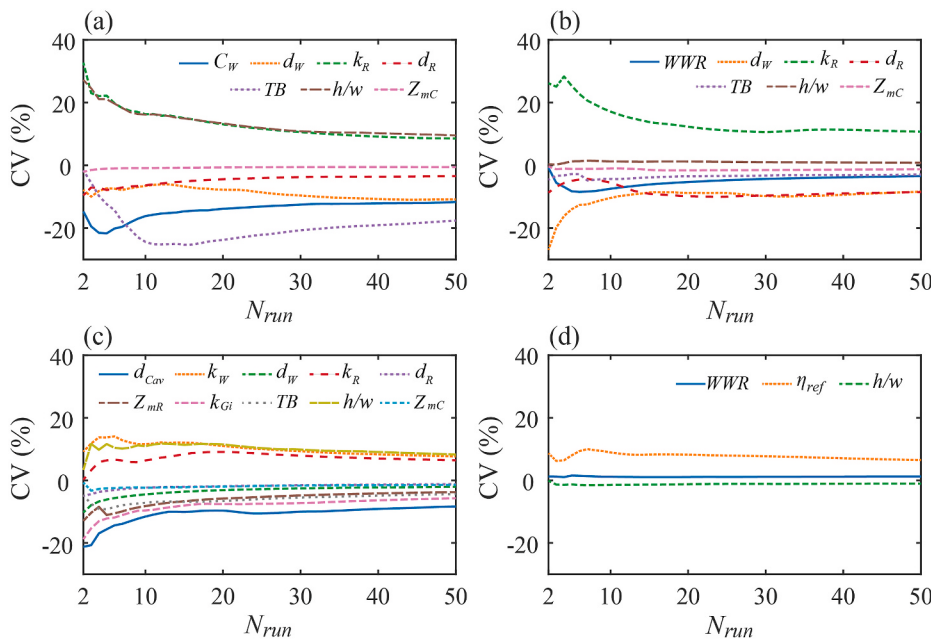


Fig. 5. Relationship between CV of standard scores for sensitive parameters ($|SS| > 0.15$) and the number of independent runs for monitored output (a) T_{can}^{max} , (b) T_{can}^{min} , (c) CL_{tot} , and (d) P_{tot} . The meaning of individual parameters can be found in Table 1.

43.8°C, 47.0°C, and 50.5°C, respectively (Fig. 6a). Within the uncertain parameter space, T_{can}^{max} shows a large variation from 38.1°C to 50.5°C on the simulated day. A T_{can}^{max} of 50°C presents devastating challenges to human health and electricity transmission systems [49,50], and cities shall implement proper urban heat mitigation strategies for such extreme temperatures. Fig. 6b shows that T_{can}^{min} also increases remarkably from 31.1°C with an exceedance probability of 30% to 35.2°C with a probability of 2.7%. The slope of increment in T_{can}^{min} is smaller than that of T_{can}^{max} , as daily minimum temperature occurs at night in absence of solar radiation. Exposure to warm nights nevertheless makes important contributions to heat-related mortality [51], and nocturnal heat islands require serious attention. Building cooling load CL_{tot} significantly varies with the uncertain input parameters, ranging from 43.9 kWh to 258.7 kWh (Fig. 6c). Power generation by BIPV window has a linear relationship with the exceedance probability in the semi-log plot Fig. 6d. The maximum P_{tot} reaches 30.2 kWh for the exceedance probability of 2.7%, which can offset more than 10% of the maximum daily building cooling load 258.6 kWh. Under the optimal power generation condition, the difference of indoor cooling load between buildings without window and buildings with BIPV windows is 74.71 kWh. With the coefficient of performance varies from 2.3 to 3.5 for typical air conditioning systems, the additional cooling load requires 21.35–32.48 kWh electrical energy. The maximum power generation by BIPV windows therefore can mostly offset the additional cooling energy consumption caused by replacing wall materials with BIPV window. And it is worth mentioning that energy savings will be substantially higher when BIPV windows are employed to replace traditional clear glass windows in cooling-dominated low latitude cities, as reported in previous simulation studies [20–23].

Different profiles of the four monitor outputs in Fig. 6 implies the different mechanisms that regulate the outdoor temperature, building energy consumption, and renewable energy generation in the built environment. It is noteworthy that the variation in P_{tot} between individual runs (grey lines in Fig. 6) is the largest among four monitored outputs. And the maximum P_{tot} of 30.2 kWh with an exceedance probability of 2.7% is about three times the value of 8.8 kWh with an exceedance probability of 30%. This emphasizes the importance of accurate estimation of input parameters: uncertainties can lead to a vast variation in the BIPV window benefit in the built environment,

especially under rare conditions of low frequency.

3.3. Sensitivity to uncertain parameters

We then looked into the key parameters that regulate the response of four monitored outputs. The sensitivity of individual outputs to studied input parameters is estimated through the standard score, which is summarized in Table 2. As shown in Table 2 column (1), among all parameters, T_{can}^{max} is extremely sensitive to Z_{mc} ($|SS| \geq 0.75$), very sensitive to d_R ($|SS| \geq 0.5$), and slightly sensitive to d_w , C_w , h/w , k_R , and TB ($|SS| \geq 0.15$). Other parameters, especially the BIPV window-related parameters, play insignificant roles in increasing T_{can}^{max} with $|SS| < 0.15$. The roughness length of momentum above canyon Z_{mc} is a crucial factor controlling the turbulent heat dispersion from canyon to overlying atmosphere. Small Z_{mc} leads to a reduced efficiency of canyon heat dispersion, and thus the SS of Z_{mc} is -1.32 for T_{can}^{max} . Considerable sensitivity of T_{can}^{max} to roof thickness d_R is different from the finding in the previous study [36]. When building energy simulation was not considered, rooftop properties were found uncorrelated with canyon air temperature. In this study, we find that though rooftop material does not directly interact with canyon air, its impact on building cooling load can indirectly modify the canyon thermal environment. Thinner roof materials with larger thermal conductivity facilitate heat transfer indoor, leading to higher CL_{tot} (CL_{tot} sensitive to d_R and k_R in Table 2 column (3)) and subsequently more waste heat released to warm the canyon. As a result, the SS of d_R and k_R for T_{can}^{max} is -0.55 and 0.15 , respectively. In terms of wall materials, only wall thickness d_w and heat capacity C_w have a slightly negative impact on maximizing T_{can}^{max} . This further suggests that good thermal insulation of building envelope is important for mitigating extreme urban heat in the built environment. Regarding the morphological parameters, street canyon with a higher aspect ratio (h/w) can trap more incoming solar radiation through multiple reflections between buildings, and better retain building waste heat in the canyon atmosphere by reducing advective heat transfer, which tend to increase T_{can} during the day. At the same time, a higher aspect ratio leads to stronger shading effect on buildings and thus reduction of daytime T_{can} . Under the clear sky condition in Phoenix, the SS of h/w for T_{can}^{max} is 0.17 , suggesting that the trapping effect plays a more important role and T_{can}^{max} increases with the canyon aspect ratio. Note that

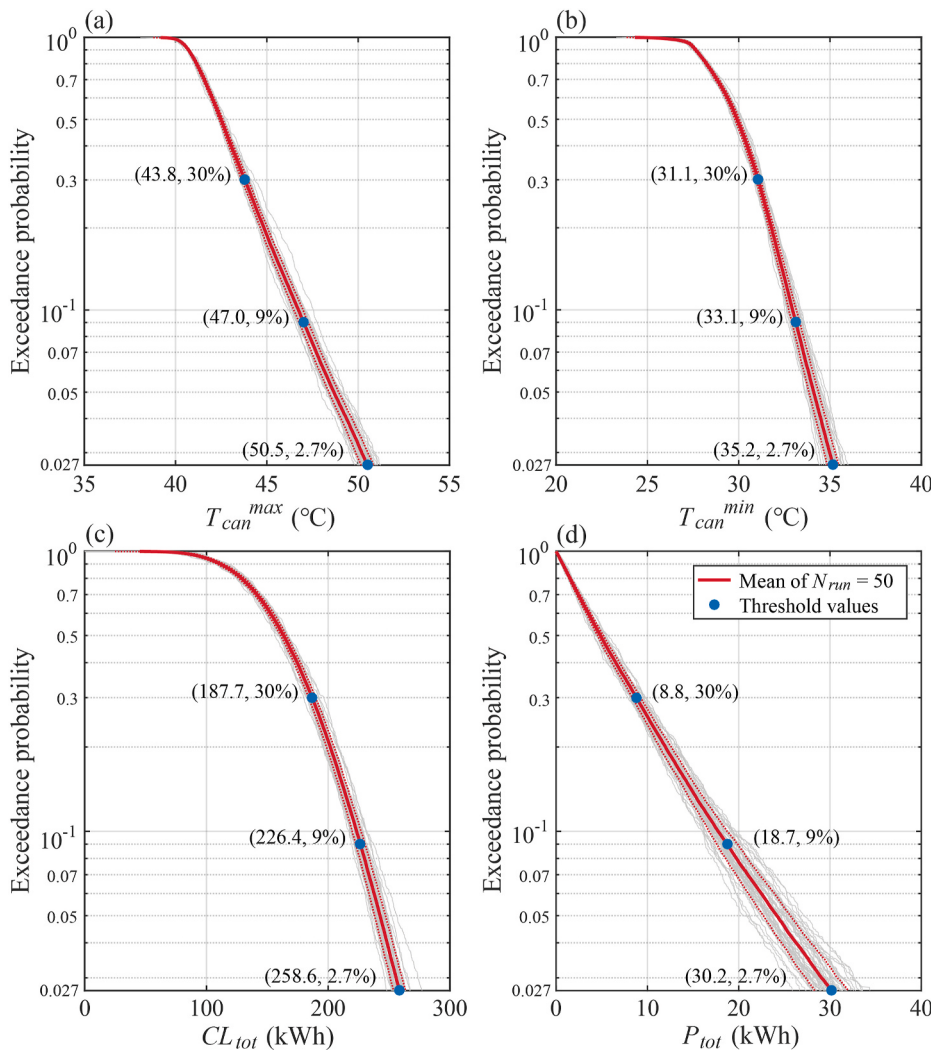


Fig. 6. Profiles of monitored output (a) T_{can}^{max} , (b) T_{can}^{min} , (c) CL_{tot} , and (d) P_{tot} at different exceedance probabilities. The dashed red line shows one standard deviation ($\pm 1\sigma$) from the mean of 50 independent runs. The grey lines show the results of individual runs. (For interpretation of the references to colour in this figure legend, the reader is referred to the Web version of this article.)

Table 2

Standard score of studied uncertain parameters for four monitored outputs. Sensitive parameters are highlighted: positive values greater than 0.15 in red, and negative values smaller than -0.15 in blue. A positive (negative) SS implies that increasing the value of input parameter results in an increase (decrease) of the monitored output.

Parameters	T_{can}^{max} (1)	T_{can}^{min} (2)	CL_{tot} (3)	P_{tot} (4)	Parameters	T_{can}^{max} (1)	T_{can}^{min} (2)	CL_{tot} (3)	P_{tot} (4)
WWR	0.13	-0.50	-0.05	0.95	a_w	-0.04	-0.04	-0.05	0.02
W_{WD}	0.00	0.01	0.01	0.03	k_w	-0.05	0.08	0.20	-0.02
H_{WD}	-0.02	0.00	-0.13	-0.01	C_w	-0.18	0.01	-0.06	-0.01
d_{PV}	0.03	0.02	-0.01	-0.01	d_w	-0.25	-0.16	-0.67	-0.01
d_{Cav}	-0.01	0.00	-0.16	-0.01	a_R	-0.02	-0.05	-0.10	0.00
d_{cg}	0.00	0.01	-0.02	-0.01	k_R	0.15	0.16	0.33	0.00
k_{PV}	0.00	-0.01	0.04	0.00	C_R	-0.07	0.02	-0.03	-0.01
k_{cg}	0.02	0.02	0.04	0.04	d_R	-0.55	-0.27	-0.81	-0.02
C_{PV}	0.00	0.01	0.03	0.00	Z_{mR}	-0.09	-0.11	-0.32	0.00
C_{cg}	0.00	0.00	-0.01	0.00	k_{Gi}	-0.08	-0.14	-0.25	0.02
ε_{PV}	-0.01	-0.02	-0.03	0.00	C_{Gi}	0.01	0.03	0.00	0.00
ε_{cg}	-0.04	-0.02	0.01	-0.01	TB	-0.15	-0.30	-0.75	-0.03
a_{PV}	0.08	-0.02	-0.06	-0.04	h/w	0.17	0.92	0.17	-0.97
a_{cg}	0.03	-0.02	0.03	0.00	θ_{can}	0.10	0.08	0.10	0.14
η_{ref}	-0.05	-0.02	-0.03	0.50	Z_{mC}	-1.32	-1.08	-0.63	-0.01
β_{ref}	0.00	0.00	0.00	-0.05					

one may expect high reflectivity or low emissivity coating for windows improve the insulating properties and retain the radiation in the outdoor environment, and as a result, daytime urban heat island increases. Results in this study, however, suggest that the influences of window emissivity and albedo on T_{can}^{max} are negligible compared to the aforementioned sensitive parameters.

Compared with T_{can}^{max} , T_{can}^{min} exhibits similar sensitivity to input parameters except for *WWR*, C_W , and *h/w* (see Table 2 column (2)). It is interesting that increased *WWR* is associated with an insignificant increase of T_{can}^{max} (*SS* = 0.13) but a significant decrease of T_{can}^{min} (*SS* = -0.50). During the daytime, buildings with larger window coverage receive more solar heat gain indoor, which reduces the amount of radiative energy for the outdoor environment and tends to mitigate daytime heat islands. Meanwhile, increased solar heat gain leads to additional waste heat released by the A/C for indoor cooling and subsequently tends to warm up the canyon air. These two mechanisms counteract each other and eventually explain the insensitive response of T_{can}^{max} to *WWR*. The result is consistent with the reported cooling of about 0.2 °C in daytime T_{can} by BIPV window in the previous simulation study [24]. After sunset, the absence of solar radiation diminishes the effect of BIPV window in redistributing the solar energy. With small heat capacity, the surface temperature of BIPV window drops rapidly due to radiative cooling, which has been observed in previous field experiments [11,52]. Later into the night, the outer surface of BIPV window becomes considerably cooler than the wall surface, and could yield negative sensible heat flux in thermal exchange with the canyon atmosphere [53]. Increased BIPV window coverage is thus beneficial for cooling the nighttime outdoor thermal environment in Phoenix. Among all parameters, canyon aspect ratio *h/w* is the determinant parameter in elevating the T_{can}^{min} with a *SS* of 0.92, which is much larger than the *SS* of 0.17 for T_{can}^{max} . This is because compact canyon leads to strong shading and heat trapping simultaneously during daytime, and the combined effect favours a hotter street canyon. The shading effect disappears at night and the heat trapping effect by canyon morphology dominates the formation of nocturnal heat island. Results here illustrate that daytime and nighttime heat mitigations require a different effective design.

Table 2 column (3) shows that CL_{tot} is extremely sensitive to d_R and TB , very sensitive to d_W and Z_{mC} , moderately sensitive to k_R and Z_{mR} , and slightly sensitive to k_{Gi} , k_W , *h/w*, and d_{Cav} . The thickness of building envelopes, including d_R , d_W , and d_{Cav} , have negative relations with CL_{tot} through modifying the thermal insulation. The roof thickness d_R is the most sensitive parameter with a *SS* of -0.81 because the amount of heat transfer indoor through the roof outweighs that through other surfaces. Similarly, thermal conductivity of roof k_R , wall k_W , and indoor ground k_{Gi} has considerable impacts on CL_{tot} via modifying the energy exchange rate between the indoor space and surrounding environment. Among BIPV window-related parameters, increasing the thickness of air cavity is the only effective way for reducing building cooling load. The negative *SS* of Z_{mR} and Z_{mC} for CL_{tot} is because smooth surfaces inhibit turbulent heat dissipation and result in larger amount of heat transfer into buildings. As expected, lowering A/C setpoint temperature (TB) will substantially increase CL_{tot} . Building cooling load links directly with waste heat emission in the canyon that both T_{can}^{max} and T_{can}^{min} have negative relations with TB . Compared to T_{can}^{max} , T_{can}^{min} is more sensitive to TB as the waste heat from buildings is the primary energy source at night.

Table 2 column (4) shows that power generation of BIPV window P_{tot} is only sensitive to three factors, including the canyon aspect ratio *h/w* (*SS* = -0.97), *WWR* (*SS* = 0.95), and PV module's electrical efficiency η_{ref} (*SS* = 0.5). It is straightforward that larger window coverage and higher converting efficiency of PV module improve the daily power generation by BIPV window. Canyon morphology controls the amount of solar radiation incident on the window surface, and results indicate that the installation of BIPV window is more suitable in open canyon (small *h/w*). Canyon orientation, with *SS* of 0.14, indicates that the

north-south orientated canyon presents more potential to generate electricity than west-east orientated canyon. Meanwhile, when installing BIPV window on the side of buildings with sufficient solar radiation to maximize the power generation, we need to pay attention to the stronger radiation indoor and the potential to cause higher cooling load (with *SS* = 0.1 of θ_{can} for CL_{tot}).

3.4. Implications for BIPV window application

The uncertainty characterization and sensitivity analysis above can provide important guideline for BIPV window application on vertical façade and urban neighbourhood design to circumvent undesired extreme conditions. As outdoor and indoor environments are closely related, optimizing the benefit of BIPV window requires a holistic consideration of uncertain parameters. To facilitate the visualization of key factors, parameters with $|SS| \geq 0.15$ are plotted in Fig. 7. With extensive simulations of the BIPV window effect in a variety of street canyons, the following recommendations can be drawn from our analyses: (1) Increasing BIPV window coverage in open neighbourhoods (small *h/w*) is the most effective way to enlarge renewable energy share in the built environment, and can substantially alleviate nocturnal heat islands (consistent with the findings of cooling effect of PV panel deployment in cities in hot arid climates [54]). This implies that BIPV window shall be installed on buildings away from each other to avoid mutual shading. (2) For BIPV window manufacturers, the conversion efficiency of PV module is the paramount factor to improve the competitiveness of their products, and a thicker air cavity layer is useful for reducing the daily building cooling load. (3) Building envelope with good thermal insulation can remarkably cut the daily cooling demand. The thickness and thermal conductivity of wall and roof materials have a much larger impact on building energy efficiency than the canyon morphology. And hence a proper usage of construction materials is of great importance. (4) A higher A/C setpoint temperature leads to the co-benefit of reducing cooling load and cooling the outdoor environment. As the setpoint temperature is directly associated with residents' preference, understanding the occupant behaviours in different climate regions and shaping them towards a sustainable way is worthy of further investigation [55,56]. (5) Momentum roughness length above canyon is critical in mitigating the extreme temperatures and building cooling loads in the built environment. Landscape layout and building design that facilitates heat dispersion out of urban neighbourhoods shall be prioritized for reducing the risk of extreme heat. (6) Though daily maximum temperature and daily minimum temperature is correlated, the effectiveness of strategies in mitigating daytime and nighttime urban heat is different. Urban planner and decision makers shall account for the diurnal population pattern into the implementation of heat mitigation strategy in different neighbourhoods. It is worth mentioning that PV panels are the most effective in receiving solar radiation when deployed on building rooftops. The recommendations above only apply to BIPV windows on vertical façades, and rooftop BIPV applications can be explored in future study.

4. Concluding remarks

In this study, the uncertainty and sensitivity of the BIPV window effect in the built environment is investigated through the coupled BEM-SLUCM model using an advanced Markov chain Monte Carlo algorithm. Responses of T_{can}^{max} , T_{can}^{min} , CL_{tot} , and P_{tot} are monitored to quantify the BIPV window impact on outdoor microclimate and building energy efficiency at the neighbourhood scale. The ranking of the uncertain parameters from the sensitivity analysis demonstrates their relative impacts on modifying the four monitored outputs. Results show that canyon aspect ratio, window coverage, and power generation efficiency play important roles in determining the power generation of BIPV window. Large BIPV window coverage can help reduce T_{can}^{min} and thus mitigate nocturnal urban heat island during summertime in Phoenix, but

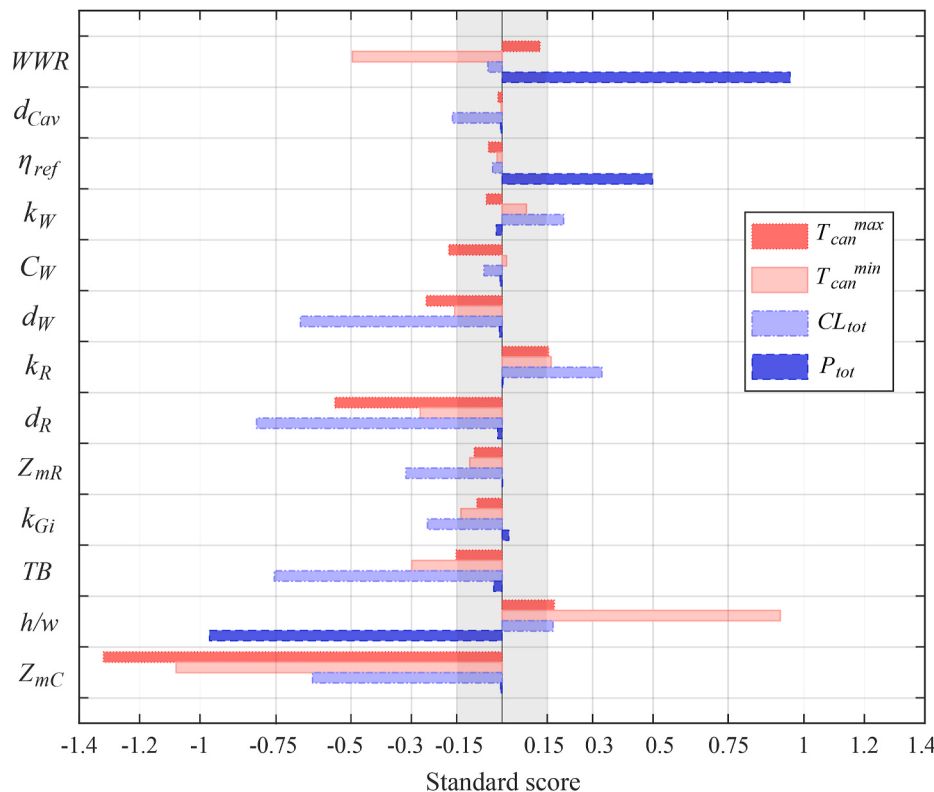


Fig. 7. Standard score of sensitive parameters for monitored output T_{can}^{max} , T_{can}^{min} , CL_{tot} , and P_{tot} . The shaded area defines the threshold (-0.15 to 0.15) above which parameters are considered as sensitive.

not T_{can}^{max} in the day. A thick air cavity layer is capable of reducing the heat transfer through BIPV window and lowering the daily cooling load of buildings. Such insulation effect can be further enhanced through the latest vacuum glazing technology, e.g., vacuum photovoltaic insulated glass unit [57]. In contrast, optical and thermal properties of BIPV window have relatively insignificant influences on four monitored outputs. Though focused on the BIPV window impact, our analyses also reveal other key parameters in affecting the outdoor microclimate and building cooling load. Thermal insulation by building envelopes is a key process that regulates the indoor-outdoor heat exchange, and T_{can} and CL_{tot} exhibit strong sensitivity to the thermal conductivity and thickness of roof and wall materials. The A/C setpoint temperature has considerable influences in modulating CL_{tot} , which subsequently determines the energy budgets of street canyon especially during nighttime. The momentum roughness length above canyon plays the most crucial role in regulating the vertical energy transport from canyon to above atmosphere, and thus has the strongest effect on creating extreme consequences.

We would like to emphasize here that results of sensitivity analysis are based on the BEM-SLUCM numerical framework, which focuses on the non-ventilated amorphous silicon BIPV window impact at the neighbourhood scale. Readers shall refer to the previous study [24] for the benefit of BIPV windows in urban canyons in comparison against clear windows. The MCMC algorithm can be an effective approach to quantify the uncertainty and sensitivity of other advanced BIPV window technologies in the future, e.g., PV-vacuum glazing [57] and Building-integrated photovoltaic/thermal (BIPVT) system [58]. The uncertain parameters analysed in this study cover a wide range of feasible values that represent a variety of urban neighbourhoods. The findings therefore provide useful guidance for BIPV window applications for city planners. In addition, the statistical quantification of sensitivity can effectively save time in parameter calibration procedures of urban canopy models to yield better predictions. For BIPV window

applications at the building scale, such as the incorporation of real-/specific buildings into the optimal location design for BIPV window, the current modelling framework is incapable and further development is required for three-dimensional modelling [59,60]. Our simulations were conducted for one sunny summer day in the desert city Phoenix, sensitivity and uncertainty of the BIPV window effect under different weather conditions in other cities shall be explored in the future.

Declaration of competing interest

The authors declare that they have no known competing financial interests or personal relationships that could have appeared to influence the work reported in this paper.

Acknowledgement

This work was supported by the National Natural Science Foundation of China (42005076).

References

- [1] United Nations, Department of Economic and Social Affairs, Population Division, *World Urbanization Prospects: the 2018 Revision*, ST/ESA/SER.A/420, New York, 2019.
- [2] International Energy Agency, *Tracking buildings 2020*, Paris. <https://www.iea.org/reports/tracking-buildings-2020>, 2020.
- [3] United Nations Environment Programme, *2020 Global Status Report for Buildings and Construction: towards a Zero-Emission, Efficient and Resilient Buildings and Construction Sector*, 2020. Nairobi.
- [4] G. Masson, I. Kaizuka, *Trends in Photovoltaic Application 2020*, International Energy Agency, 2020.
- [5] A. Kylli, P.A. Fokaides, *Investigation of building integrated photovoltaics potential in achieving the zero energy building target*, *Indoor Built Environ.* 23 (2014) 92–106.
- [6] The European Parliament and the Council of the European Union, Directive 2010/31/EU of the European Parliament and of the Council of 19 May 2010 on the Energy Performance of Buildings (Recast), Official Journal of the European Union, 2010, pp. L153/13–35.

- [7] International Energy Agency, Renewable energy market Update 2021, Paris, <http://www.iea.org/reports/renewable-energy-market-update-2021>, 2021.
- [8] G. Kavlak, J. Mcnerney, J.E. Trancik, Evaluating the causes of cost reduction in photovoltaic modules, *Energy Pol.* 123 (2018) 700–710.
- [9] International Energy Agency, Renewables 2020, Paris, <https://www.iea.org/reports/renewables-2020>, 2020.
- [10] A. Ghosh, Potential of building integrated and attached/applied photovoltaic (BIPV/BAPV) for adaptive less energy-hungry building's skin: a comprehensive Review, *J. Clean. Prod.* (2020) 123343.
- [11] J.-H. Yoon, S.-R. Shim, Y.S. An, K.H. Lee, An experimental study on the annual surface temperature characteristics of amorphous silicon BIPV window, *Energy Build.* 62 (2013) 166–175.
- [12] C.-H. Young, Y.-L. Chen, P.-C. Chen, Heat insulation solar glass and application on energy efficiency buildings, *Energy Build.* 78 (2014) 66–78.
- [13] S. Yang, A. Cannavale, D. Prasad, A. Sproul, F. Fiorito, Numerical Simulation Study of BIPV/T Double-Skin Facade for Various Climate Zones in Australia: Effects on Indoor Thermal Comfort, *Building Simulation*, Springer, 2019, pp. 51–67.
- [14] J. Peng, L. Lu, H. Yang, An experimental study of the thermal performance of a novel photovoltaic double-skin facade in Hong Kong, *Sol. Energy* 97 (2013) 293–304.
- [15] A. Ghosh, N. Sarmah, S. Sundaram, T.K. Mallick, Numerical studies of thermal comfort for semi-transparent building integrated photovoltaic (BIPV)-vacuum glazing system, *Sol. Energy* 190 (2019) 608–616.
- [16] C. Qiu, H. Yang, W. Zhang, Investigation on the Energy Performance of a Novel Semi-transparent BIPV System Integrated with Vacuum Glazing, *Building Simulation*, Springer, 2019, pp. 29–39.
- [17] A. Virtuani, D. Strepparava, Modelling the performance of amorphous and crystalline silicon in different typologies of building-integrated photovoltaic (BIPV) conditions, *Sol. Energy* 146 (2017) 113–118.
- [18] H.J. An, J.H. Yoon, Y.S. An, E. Heo, Heating and cooling performance of office buildings with a-Si BIPV windows considering operating conditions in temperate climates: the case of Korea, *Sustainability* 10 (2018) 4856.
- [19] L. Lu, K.M. Law, Overall energy performance of semi-transparent single-glazed photovoltaic (PV) window for a typical office in Hong Kong, *Renew. Energy* 49 (2013) 250–254.
- [20] Y.T. Chae, J. Kim, H. Park, B. Shin, Building energy performance evaluation of building integrated photovoltaic (BIPV) window with semi-transparent solar cells, *Appl. Energy* 129 (2014) 217–227.
- [21] W. Liao, S. Xu, Energy performance comparison among see-through amorphous-silicon PV (photovoltaic) glazings and traditional glazings under different architectural conditions in China, *Energy* 83 (2015) 267–275.
- [22] S.L. Do, M. Shin, J.-C. Baltazar, J. Kim, Energy benefits from semi-transparent BIPV window and daylight-dimming systems for IECC code-compliance residential buildings in hot and humid climates, *Sol. Energy* 155 (2017) 291–303.
- [23] T. Salameh, M.E.H. Assad, M. Tawalbeh, C. Ghenai, A. Merabet, H.F. Öztop, Analysis of cooling load on commercial building in UAE climate using building integrated photovoltaic façade system, *Sol. Energy* 199 (2020) 617–629.
- [24] L. Chen, X. Zheng, J. Yang, J.H. Yoon, Impact of BIPV windows on building energy consumption in street canyons: model development and validation, *Energy Build.* (2021) 111207.
- [25] J. Yang, Z.-H. Wang, Physical parameterization and sensitivity of urban hydrological models: application to green roof systems, *Build. Environ.* 75 (2014) 250–263.
- [26] J. Yang, Z.-H. Wang, Optimizing urban irrigation schemes for the trade-off between energy and water consumption, *Energy Build.* 107 (2015) 335–344.
- [27] C. Wang, Z.-H. Wang, Y.-H. Ryu, A single-layer urban canopy model with transmissive radiation exchange between trees and street canyons, *Build. Environ.* 191 (2021) 107593.
- [28] P. Li, Z.-H. Wang, Modeling carbon dioxide exchange in a single-layer urban canopy model, *Build. Environ.* 184 (2020) 107243.
- [29] J. Yang, Z. Wang, K.E. Kaloush, H. Dylla, Effect of pavement thermal properties on mitigating urban heat islands: a multi-scale modeling case study in Phoenix, *Build. Environ.* 108 (2016) 110–121.
- [30] Y.H. Ryu, E. Bou-Zeid, Z. Wang, J.A. Smith, Realistic representation of trees in an urban canopy model, *Boundary-Layer Meteorol.* 159 (2016) 193–220.
- [31] F. Salamanca, A. Krp, A. Martilli, A. Clappier, A new building energy model coupled with an urban canopy parameterization for urban climate simulations—part I. formulation, verification, and sensitivity analysis of the model, *Theor. Appl. Climatol.* 99 (2010) 331.
- [32] J. Teixeira, J. Fallmann, A. Carvalho, A. Rocha, Surface to boundary layer coupling in the urban area of Lisbon comparing different urban canopy models in WRF, *Urb. Clim.* 28 (2019) 100454.
- [33] T. Loridan, C. Grimmond, S. Grossman-Clarke, F. Chen, M. Tewari, K. Manning, A. Martilli, H. Kusaka, M. Best, Trade-offs and responsiveness of the single-layer urban canopy parametrization in WRF: an offline evaluation using the MOSCEM optimization algorithm and field observations, *Q. J. R. Meteorol. Soc.* 136 (2010) 997–1019.
- [34] S.-K. Au, J.L. Beck, Estimation of small failure probabilities in high dimensions by subset simulation, *Probabilist. Eng. Mech.* 16 (2001) 263–277.
- [35] P. Li, Z.-H. Wang, Uncertainty and Sensitivity Analysis of Modeling Plant CO₂ Exchange in the Built Environment, *Building and Environment*, 2020, p. 107539.
- [36] Z.-H. Wang, E. Bou-Zeid, S.K. Au, J.A. Smith, Analyzing the sensitivity of WRF's single-layer urban canopy model to parameter uncertainty using advanced Monte Carlo simulation, *J. Appl. Meteorol. Climatol.* 50 (2011) 1795–1814.
- [37] M. Montecchi, P. Polato, Simple equations to predict the daylighting behaviour of glazing by normal incidence spectrophotometry, *Rivista della Staz. Sper. Vetro* 5 (1995) 165–173.
- [38] J.-H. Song, Y.-S. An, S.-G. Kim, S.-J. Lee, J.-H. Yoon, Y.-K. Choung, Power output analysis of transparent thin-film module in building integrated photovoltaic system (BIPV), *Energy Build.* 40 (11) (2008) 2067–2075.
- [39] D.L. Evans, L.W. Florschuetz, Cost studies on terrestrial photovoltaic power systems with sunlight concentration, *Sol. Energy* 19 (1977) 255–262.
- [40] E. Skoplaki, J.A. Palyvos, On the temperature dependence of photovoltaic module electrical performance: a review of efficiency/power correlations, *Sol. Energy* 83 (2009) 614–624.
- [41] K. Bücher, G. Kleiss, D. Dätzner, Photovoltaic modules in buildings: performance and safety, *Renew. Energy* 15 (1998) 545–551.
- [42] E. Cuce, P.M. Cuce, Optimised performance of a thermally resistive PV glazing technology: an experimental validation, *Energy Rep.* 5 (2019) 1185–1195.
- [43] H.-Y. Chen, C. Chen, Determining the emissivity and temperature of building materials by infrared thermometer, *Construct. Build. Mater.* 126 (2016) 130–137.
- [44] G. Ban-Weiss, C. Wray, W. Delp, P. Ly, H. Akbari, R. Levinson, Electricity production and cooling energy savings from installation of a building-integrated photovoltaic roof on an office building, *Energy Build.* 56 (2013) 210–220.
- [45] I.D. Stewart, T.R. Oke, Local climate zones for urban temperature studies, *Bull. Am. Meteorol. Soc.* 93 (2012) 1879–1900.
- [46] D.F. Nadeau, W. Brutsaert, M. Parlange, E. Bou-Zeid, G. Barrenetxea, O. Couach, M.-O. Boldi, J.S. Selker, M. Vetterli, Estimation of urban sensible heat flux using a dense wireless network of observations, *Environ. Fluid Mech.* 9 (2009) 635–653.
- [47] W.T. Chow, T.J. Volo, E.R. Vivoni, G.D. Jenerette, B.L. Ruddell, Seasonal dynamics of a suburban energy balance in Phoenix, Arizona, *Int. J. Climatol.* 34 (2014) 3863–3880.
- [48] C.S.B. Grimmond, M. Blackett, M. Best, J. Barlow, J. Baik, S. Belcher, S. Bohnenstengel, I. Calmet, F. Chen, A. Dandou, The international urban energy balance models comparison project: first results from phase 1, *J. Appl. Meteorol. Climatol.* 49 (2010) 1268–1292.
- [49] J. Tan, Y. Zheng, X. Tang, C. Guo, L. Li, G. Song, X. Zhen, D. Yuan, A.J. Kalkstein, F. Li, The urban heat island and its impact on heat waves and human health in Shanghai, *Int. J. Biometeorol.* 54 (2010) 75–84.
- [50] N.L. Miller, K. Hayhoe, J. Jin, M. Aufhammer, Climate, extreme heat, and electricity demand in California, *J. Appl. Meteorol. Climatol.* 47 (2008) 1834–1844.
- [51] P. Murage, S. Hajat, R.S. Kovats, Effect of night-time temperatures on cause and age-specific mortality in London, *Environ. Epidemiol.* 1 (2017), e005.
- [52] W. Zhang, B. Hao, N. Li, Experiment and simulation study on the amorphous silicon photovoltaic walls, *Int. J. Photoenergy* (2014) 643637.
- [53] J.V. Pham, A. Baniassadi, K.E. Brown, J. Heusinger, D.J. Sailor, Comparing photovoltaic and reflective shade surfaces in the urban environment: effects on surface sensible heat flux and pedestrian thermal comfort, *Urb. Clim.* 29 (2019) 100500.
- [54] F. Salamanca, M. Georgescu, A. Mahalov, M. Moustaqui, A. Martilli, Citywide impacts of cool roof and rooftop solar photovoltaic deployment on near-surface air temperature and cooling energy demand, *Boundary-Layer Meteorol.* 161 (2016) 203–221.
- [55] F.D. Salim, B. Dong, M. Ouf, Q. Wang, I. Pigliautile, X. Kang, T. Hong, W. Wu, Y. Liu, S.K. Rumi, Modelling urban-scale occupant behaviour, mobility, and energy in buildings: a survey, *Build. Environ.* 183 (2020) 106964.
- [56] C.S. Hayles, M. Dean, Social housing tenants, Climate Change and sustainable living: a study of awareness, behaviours and willingness to adapt, *Sustain. Cities Soc.* 17 (2015) 35–45.
- [57] A. Ghosh, S. Sundaram, T.K. Mallick, Investigation of thermal and electrical performances of a combined semi-transparent PV-vacuum glazing, *Appl. Energy* 228 (2018) 1591–1600.
- [58] H.M. Maghrabie, K. Elsaid, E.T. Sayed, M.A. Abdelkareem, T. Wilberforce, A. Olabi, Building-integrated photovoltaic/thermal (BIPVT) systems: applications and challenges, *Sustain. Energy Technol. Assess.* 45 (2021) 101151.
- [59] S. Schubert, S. Grossman-Clarke, A. Martilli, A double-canyon radiation scheme for multi-layer urban canopy models, *Boundary-Layer Meteorol.* 145 (2012) 439–468.
- [60] A. Azami, H. Sevinç, The energy performance of building integrated photovoltaics (BIPV) by determination of optimal building envelope, *Build. Environ.* 199 (2021) 107856.